CANCER

Therapeutic targeting of the MYC signal by inhibition of histone chaperone FACT in neuroblastoma

Daniel R. Carter,[1,2]* Jayne Murray,[1]* Belamy B. Cheung,[1,2] Laura Gamble,[1] Jessica Koach,[1] Joanna Tsang,[1] Selina Sutton,[1] Heyam Kalla,[1] Sarah Syed,[1] Andrew J. Gifford,[1,3] Natalia Issaeva,[4] Asel Biktasova,[4] Bernard Atmadibrata,[1] Yuting Sun,[1] Nicolas Sokolowski,[1] Dora Ling,[1] Patrick Y. Kim,[1] Hannah Webber,[1] Ashleigh Clark,[1] Michelle Ruhle,[1] Bing Liu,[1] André Oberthuer,[5,6] Matthias Fischer,[5,7] Jennifer Byrne,[8,9] Federica Saletta,[8] Le Myo Thwe,[8,9] Andrei Purmal,[10] Gary Haderski,[11] Catherine Burkhart,[11] Frank Speleman,[12] Katleen De Preter,[12] Anneleen Beckers,[12] David S. Ziegler,[1,2,13] Tao Liu,[12] Katerina V. Gurova,[10,14] Andrei V. Gudkov,[10,14] Murray D. Norris,[1,15] Michelle Haber,[1†] Glenn M. Marshall[1,13†]

Amplification of the *MYCN* oncogene predicts treatment resistance in childhood neuroblastoma. We used a MYC target gene signature that predicts poor neuroblastoma prognosis to identify the histone chaperone FACT (facilitates chromatin transcription) as a crucial mediator of the MYC signal and a therapeutic target in the disease. FACT and MYCN expression created a forward feedback loop in neuroblastoma cells that was essential for maintaining mutual high expression. FACT inhibition by the small-molecule curaxin compound CBL0137 markedly reduced tumor initiation and progression in vivo. CBL0137 exhibited strong synergy with standard chemotherapy by blocking repair of DNA damage caused by genotoxic drugs, thus creating a synthetic lethal environment in *MYCN*-amplified neuroblastoma cells and suggesting a treatment strategy for MYCN-driven neuroblastoma.

INTRODUCTION

Neuroblastoma is a pediatric cancer of the sympathetic nervous system, which often presents at a clinically advanced stage with primary or acquired resistance to conventional chemotherapy (*1*, *2*). Amplification of the *c-MYC* homolog *MYCN* is observed in ~15 to 20% of patients (*3*, *4*), and this feature strongly correlates with poor clinical outcome (*1*, *2*). Direct evidence of *MYCN* as an oncogene is highlighted by the *TH-MYCN* mouse model, in which a *MYCN* transgene driven by the tyrosine hydroxylase (*TH*) promoter is sufficient to recapitulate many of the features of human neuroblastoma (*5*). In addition to *MYCN* amplification being an effective biomarker for poor prognosis in high-risk neuroblastoma patients, it has also been reported that increased activation of MYC transcriptional target genes predicts poor prognosis in clinical stage 4 patients, independently of *MYCN* amplification (*6*). Paradoxically, these patients had very low expression of MYCN, suggesting that c-MYC, the expression of which is inversely correlated to MYCN, acts in a functionally redundant manner for MYC-directed transcription (*6*). Thus, targeting genes downstream of MYC proteins may be an alternative therapeutic strategy for high-risk neuroblastoma patients.

Here, we used a prognostic MYC target gene signature to identify the histone chaperone FACT (facilitates chromatin transcription) as a promising therapeutic target in neuroblastoma. We found that FACT and MYCN expression act in a positive feedback regulatory loop in neuroblastoma cells, are strongly correlated during tumor initiation, and result in a remarkable susceptibility of neuroblastoma cells to the FACT inhibitor CBL0137. Moreover, because of the role of FACT in DNA repair, CBL0137 created a synthetic lethal environment when combined with genotoxic chemotherapy, suggesting a promising treatment approach for this aggressive childhood malignancy.

RESULTS

A MYC target gene signature identifies the histone chaperone FACT as a prognostic marker in neuroblastoma

To identify MYC target genes as therapeutic targets in neuroblastoma, we examined the expression of a previously reported MYC core target gene signature (*7*) in neuroblastoma tumors derived from patients at primary diagnosis. We conducted an unsupervised hierarchical clustering on 649 neuroblastoma patients (*4*), and as expected, this identified not only marked up-regulation in a cluster that corresponded to *MYCN*-amplified tumors (MYCN-amplified cluster) but also high expression in some *MYCN*-nonamplified tumors (MYC activation cluster) (Fig. 1A). The MYC activation cluster was associated with indicators of poor prognosis, including older patient age (>18 months) or

[1]Children's Cancer Institute Australia, Lowy Cancer Research Centre, University of New South Wales, Randwick, New South Wales 2031, Australia. [2]School of Women's and Children's Health, UNSW Australia, Randwick, New South Wales 2031, Australia. [3]Department of Anatomical Pathology (SEALS), Prince of Wales Hospital, Randwick, New South Wales 2031, Australia. [4]Department of Surgery, Otolaryngology, and Yale Cancer Center, Yale University, New Haven, CT 06511, USA. [5]Department of Pediatric Oncology and Hematology, Children's Hospital, University of Cologne, 50931 Cologne, Germany. [6]Department of Neonatology and Pediatric Intensive Care Medicine, Children's Hospital, University of Cologne, 50931 Cologne, Germany. [7]Max Planck Institute for Metabolism Research, 50931 Cologne, Germany. [8]Children's Cancer Research Unit, Kids Research Institute, The Children's Hospital at Westmead, Locked Bag 4001, Westmead, New South Wales 2145, Australia. [9]University of Sydney Discipline of Paediatrics and Child Health, The Children's Hospital at Westmead, Locked Bag 4001, Westmead, New South Wales 2145, Australia. [10]Incuron, LLC, Buffalo, NY 14203, USA. [11]Buffalo BioLabs, LLC, Buffalo, NY 14203, USA. [12]Center for Medical Genetics (CMGG), Ghent University, Medical Research Building (MRB1), De Pintelaan 185, 9000 Ghent, Belgium. [13]Kids Cancer Centre, Sydney Children's Hospital, Randwick, New South Wales 2031, Australia. [14]Department of Cell Stress Biology, Roswell Park Cancer Institute, Elm and Carlton Streets, Buffalo, NY 14263, USA. [15]University of New South Wales Centre for Childhood Cancer Research, Randwick, New South Wales 2031, Australia.
*These authors are co-first authors.
†Corresponding author. E-mail: g.marshall@unsw.edu.au (G.M.M.); mhaber@ccia.unsw.edu.au (M.H.)

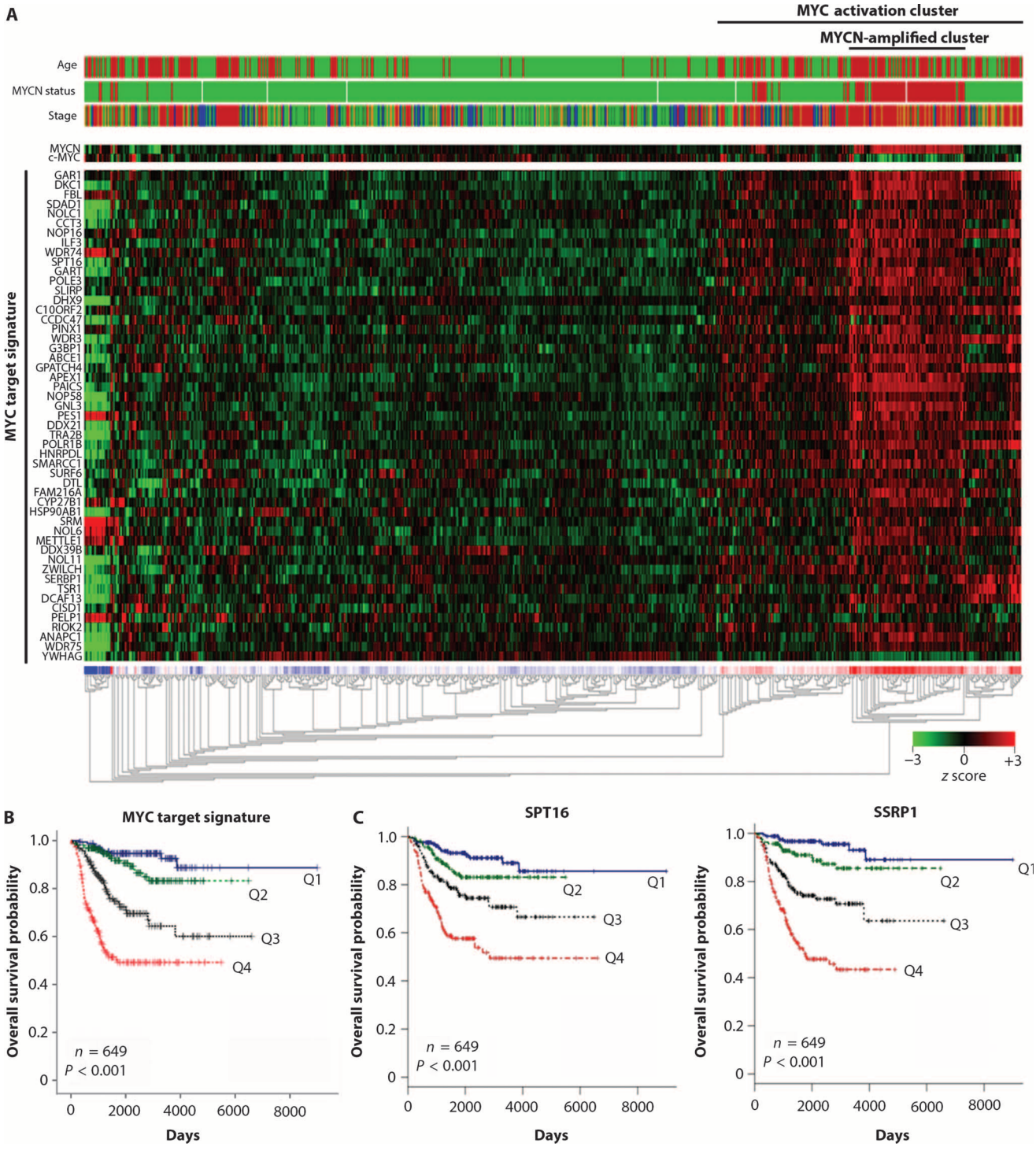

Fig. 1. FACT predicts poor prognosis in neuroblastoma patients and is associated with MYC signaling. (**A**) Unsupervised hierarchical clustering on 649 neuroblastoma patients according to a 51-gene MYC target signature (*7*). Clinical parameters (top) were included as follows: patient age (>18 months: red; <18 months: green), MYCN amplification status (amplified: red; nonamplified: green), and International Neuroblastoma Staging System (stage 1 + 2: green; stage 3: orange; stage 4: red; stage 4S: blue). Clustering was performed according to the Euclidean distance using the R2 microarray analysis and visualization platform (http://r2.amc.nl). (**B**) Kaplan-Meier plots for overall survival of 649 neuroblastoma patients stratified by expression quartiles of the MYC target signature. MYC target signature expression quartiles were generated by averaging the expression of all 51 gene members of the MYC signature per patient and ranking from lowest to highest: Q1, 0 to 25th patient percentile; Q2, 25th to 50th patient percentile; Q3, 50th to 75th patient percentile; and Q4, 75th to 100th patient percentile. *P* value, pairwise log-rank tests on Q1 versus Q4, Q2 versus Q4, or Q3 versus Q4. See table S7 for individual *P* values. (**C**) Kaplan-Meier plots for overall survival of 649 neuroblastoma patients stratified by expression quartiles of SPT16 (left) and SSRP1 (right) as for (B) above.

advanced clinical stage 3 or 4, and the MYC target signature as a whole strongly predicted poor overall and event-free survival (Fig. 1, A and B, and fig. S1A). Next, we examined each gene member of the MYC activation signature by Cox proportional hazards modeling for prognostic significance using either (i) univariate analysis, (ii) multivariate analysis considering *MYCN* amplification status, or (iii) multivariate analysis considering *MYCN* amplification status, patient age, and stage (table S1). Eleven of 51 genes were found to be significant predictors of poor prognosis in all three analyses (table S1). Among these 11 candidates, we sought a MYC-regulated target with a clinically relevant and strong chemical inhibitor and preclinical/clinical evidence for a role in cancer (table S2). Suppressor of Ty 16 (*SUPT16H*; hereafter referred to as SPT16) was the only gene that conformed to these criteria. Together with structure-specific recognition protein 1 (SSRP1), SPT16 comprises the histone chaperone heterodimer complex FACT (*8*, *9*), which has been identified as a potential therapeutic target in a number of cancer models (*10*–*12*). Curaxin class compounds, including the lead compound CBL0137, are potent inhibitors of FACT that deplete free FACT from the soluble fraction of the nucleus, functionally reducing FACT regulation of chromatin (*12*). CBL0137 exhibits potent antitumor efficacy and minimal toxicity in experimental cancer models (*12*) and is currently being tested in early-phase clinical trials (http://clinicaltrials.gov/show/NCT01905228).

SPT16 and SSRP1 are highly dependent on each other for regulation of expression and function (*13*), so we next examined the expression of SSRP1 and SPT16 in neuroblastoma tumors. Both FACT subunits were associated with poor overall and event-free survival in two cohorts of primary neuroblastoma patients (Fig. 1C and fig. S1, B and C) (*4*, *14*). Using Cox proportional hazards modeling, we found high mRNA expression of *SSRP1* and *SPT16* to be strong and independent predictors of poor prognosis by univariate analysis or when considering *MYCN* amplification status alone or combined with patient age and stage (table S3, A and B). Moreover, SPT16 and SSRP1 expression in the 649 patient tumor cohort showed a strong association with clinical parameters of poor prognosis (fig. S1, D and E), as well as a correlation with MYCN expression or average MYC target gene expression (fig. S1, F and G).

Next, we examined whether high SSRP1 protein expression was similarly associated with poor clinical outcome. We used a tissue microarray of 47 primary untreated neuroblastomas with representative prognostic indicators for neuroblastoma (fig. S1H), and we found that high SSRP1 protein expression was a strong predictor of poor prognosis (fig. S1I). With semiquantitative scoring, high SSRP1 expression was associated with *MYCN* amplification, but this comparison did not reach statistical significance (fig. S1, J and K). To confirm that SSRP1 protein expression was higher in *MYCN*-amplified tumors, we used quantitative Western blotting on 12 primary neuroblastoma tumors and showed markedly higher amounts of SSRP1 in the *MYCN*-amplified tumors (fig. S1, L and M). Moreover, high amounts of SSRP1 and SPT16 protein correlated with high MYCN or c-MYC protein expression in cultured neuroblastoma cell lines (fig. S1, N to Q).

FACT and MYCN expression are controlled in a forward feedback loop

Because SPT16 is a direct transcriptional target of c-MYC in fibrosarcoma cell lines (*7*), we hypothesized that MYCN transcriptionally regulates FACT expression in neuroblastoma cells. Consistent with this prediction, small interfering RNA (siRNA) knockdown of MYCN decreased SPT16 and SSRP1 mRNA and protein expression in *MYCN*-amplified BE(2)C and KELLY neuroblastoma cell lines (Fig. 2, A and B). Both *SPT16* and *SSRP1* gene promoters contain a MYC E-box transactivation motif ~500 base pairs upstream of their transcriptional start sites. We used chromatin immunoprecipitation assays to demonstrate enrichment of MYCN at the E-box motif of both the *SPT16* and *SSRP1*

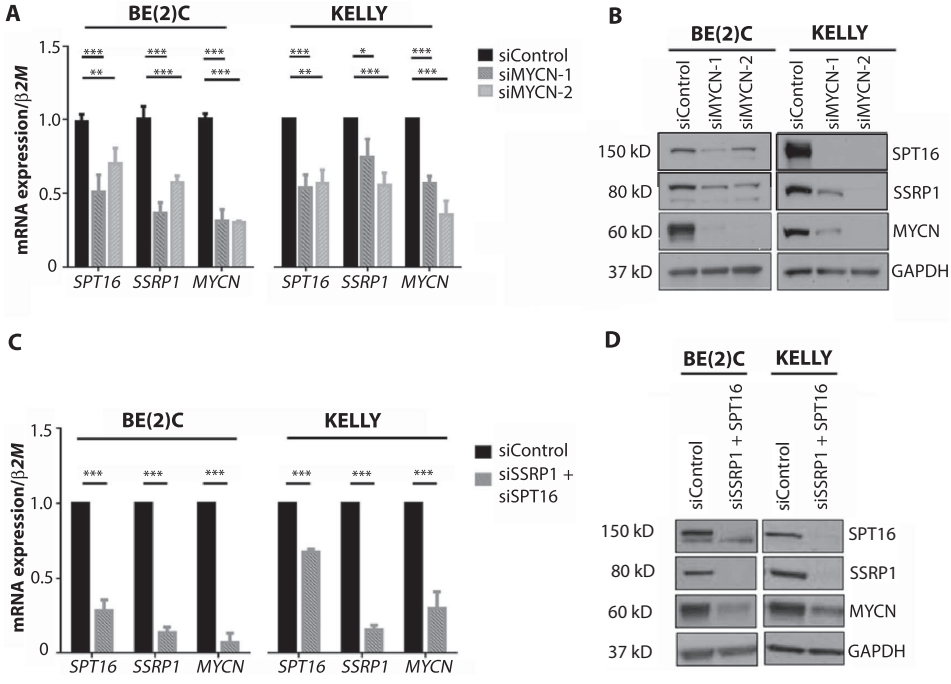

Fig. 2. FACT and MYCN act in a transcriptional positive feedback loop. (**A**) Mean mRNA expression for *SPT16*, *SSRP1*, or *MYCN* in BE(2)C and KELLY cells treated with control, MYCN-1, or MYCN-2 siRNA. Data displayed were obtained 48 hours after transfection and were normalized to mRNA expression in a control siRNA sample. β*2-Microglobulin* (β*2M*) was used as a reference gene. **P* < 0.05, ***P* < 0.01, ****P* < 0.001. See table S7 for individual *P* values. (**B**) Western blots for SPT16, SSRP1, and MYCN protein expression in BE(2)C and KELLY cells treated with control, MYCN-1, or MYCN-2 siRNA. Data displayed were obtained 48 hours after transfection. Glyceraldehyde-3-phosphate dehydrogenase (GAPDH) was used as a loading control. (**C**) Mean mRNA expression for SPT16, SSRP1, or MYCN in BE(2)C and KELLY cells treated with control or combined SSRP1 and SPT16 siRNA. Data displayed were obtained 72 hours after transfection and normalized to mRNA expression in a control siRNA sample. β*2-Microglobulin* was used as a reference gene. ****P* < 0.001. See table S7 for individual *P* values. (**D**) Western blots for SPT16, SSRP1, and MYCN protein expression in BE(2)C and KELLY cells treated with control or combined SSRP1 and SPT16 siRNA. Data displayed were obtained 72 hours after transfection. GAPDH was used as a loading control.

core promoters (fig. S2, A to C). Moreover, siRNA knockdown of MYCN reduced binding at these sites, suggesting that MYCN can transcriptionally up-regulate both FACT components. Additionally, we found that this was a general feature of MYC proteins because c-MYC siRNAs also resulted in markedly reduced protein expression of both FACT subunits in MYCN nonamplified neuroblastoma cells (fig. S2D).

FACT regulates nucleosome structure to promote transcriptional initiation and elongation (*8*, *9*). Because FACT is enriched at the *c-MYC* promoter in HT1080 fibrocarcinoma cells (*10*), we hypothesized that FACT may also enhance the transcription of *MYCN* in neuroblastoma cells, completing a forward feedback loop. Indeed, we found that siRNA knockdown of SSRP1 and SPT16 decreased *MYCN* mRNA and protein expression (Fig. 2, C and D, and fig. S2E), whereas overexpression of SSRP1 and/or SPT16 increased MYCN mRNA and protein concentrations in neuroblastoma cells (fig. S2, F and G). In addition, cycloheximide assays showed that SSRP1 or SPT16 knockdown markedly reduced MYCN protein half-life, whereas SPT16/SSRP1 overexpression prolonged the half-life of MYCN (fig. S2, H and I), suggesting that FACT regulates MYCN protein expression by two discrete mechanisms, one at the transcriptional level and the other posttranslational. This was further supported by gene set enrichment analysis, which showed a strong correlation between the pattern of altered gene expression after SSRP1 knockdown and MYCN target gene signatures (fig. S2J). Together, our data indicate a positive regulatory expression loop involving FACT and MYCN, which drives MYCN transcription and protein stability by independent mechanisms.

FACT is highly expressed in neuroblastoma precursor cells in TH-MYCN$^{+/+}$ mice

We have previously shown that high MYCN expression caused postnatal persistence and hyperplasia of neuroblasts as precancerous lesions in the developing sympathetic ganglia of *TH-MYCN* mice (*15*). Immunohistochemical analyses showed that in wild-type ganglia, SSRP1 protein expression was rapidly down-regulated after birth, whereas *TH-MYCN*$^{+/+}$ ganglia displayed high SSRP1 expression up until tumor formation at 6 weeks of age (Fig. 3A and fig. S3A). SSRP1 expression was highly correlated with MYCN expression (Fig. 3A and fig. S3, A to C), and the degree of MYCN and SSRP1 expression was highly correlated with the extent of neuroblast hyperplasia in ganglia (Fig. 3B and fig. S3, A and D to F). These results suggest that FACT is up-regulated in precancerous *TH-MYCN*$^{+/+}$neuroblasts.

FACT inhibitor CBL0137 restores developmental signals in postnatally persistent neuroblasts from TH-MYCN mice

To evaluate whether FACT is required for *TH-MYCN* neuroblast persistence and hyperplasia, we treated perinatal *TH-MYCN* mice with the FACT inhibitor CBL0137. Low-dose intraperitoneal administration of CBL0137 from 6 days of age for a total of 5 days reduced the proportion of ganglia with neuroblast hyperplasia in both hemizygote (*TH-MYCN*$^{+/-}$) and homozygote (*TH-MYCN*$^{+/+}$) mice at 2 weeks of age (Fig. 3, C and D). Furthermore, low-dose CBL0137 prophylaxis from 6 days of age until 4 weeks of age delayed subsequent tumor growth in *TH-MYCN*$^{+/+}$ mice (Fig. 3E). Histological analysis of tumors from mice given CBL0137 prophylaxis revealed an increase in ganglion-like cells within tumors (fig. S3G), suggesting that CBL0137 promoted the differentiation of neuroblasts that had pathologically persisted postnatally. Consistent with this observation, we also demonstrated that all-trans retinoic acid treatment of the human neuroblastoma cell line SH-SY5Y rapidly down-regulated expression of both SSRP1 and SPT16 (fig. S3H) at a time that coincided with terminal neuritic differentiation in vitro (*16*, *17*).

We have previously shown that MYCN blocked developmental cell deletion signals in premalignant *TH-MYCN*$^{+/+}$ ganglia cells after nerve growth factor or serum withdrawal in vitro, which mirrored postnatal neuroblast persistence and hyperplasia in vivo (*15*, *18*, *19*). To evaluate the role of FACT in neuroblast death responses, we cultured primary ganglia from 2-week-old *TH-MYCN*$^{+/+}$ mice with CBL0137. *TH-MYCN*$^{+/+}$ ganglia were more sensitive to the cytopathic effects of CBL0137 in cultures deprived of serum compared with wild-type ganglia (Fig. 3F and fig. S3I). Moreover, when 1-week-old *TH-MYCN*$^{+/+}$ mice were treated with low-dose CBL0137 for 5 days, primary ganglia cultures derived from treated mice also exhibited sensitivity to trophic factor withdrawal compared with vehicle-treated mice (fig. S3J). Together, this suggested that CBL0137 restored normal cell deletion responses to trophic factor withdrawal, despite high MYCN expression, blocking the earliest steps of this MYCN-driven embryonal cancer.

We have previously shown that p53 stress responses to trophic factor withdrawal are impaired in a MYCN-dependent manner in *TH-MYCN*$^{+/+}$ ganglia compared with wild-type ganglia (*19*). Consistent with this observation, gene set enrichment analysis identified suppression of gene sets related to p53 target genes in *TH-MYCN*$^{+/+}$ mice compared with age-matched wild-type mice (table S4). CBL0137 has previously been shown to activate p53; thus, we evaluated whether CBL0137 could restore p53 stress responses in serum-deprived *TH-MYCN*$^{+/+}$ ganglia. Rescue experiments with the p53 inhibitor pifithrin-α (PFTα) (*20*) and the pan-caspase inhibitor OPH-Q-VD demonstrated that CBL0137 sensitized *TH-MYCN*$^{+/+}$ ganglia to trophic factor withdrawal in a p53-dependent manner (fig. S3K) and required activation of caspase signaling (fig. S3L). Inactivation of p53 as the mechanism of resistance to trophic withdrawal in *TH-MYCN*$^{+/+}$ ganglia was further supported by the finding that the p53 signal activator Nutlin-3a (*21*) also restored the death responses to trophic factor withdrawal in a p53-dependent, proapoptotic manner (fig. S3, M to P).

FACT inhibition is an effective therapeutic strategy for MYCN-driven neuroblastoma

Next, we examined the impact of FACT inhibition on neuroblastoma cell viability. FACT siRNAs reduced cell viability of BE(2)C and SH-SY5Y cells, neuroblastoma cells with high expression of MYCN and c-MYC, respectively (figs. S1N and S4, A and B). Moreover, FACT siRNAs inhibited MYCN protein expression, as well as colony number increases in SHEP.MYCN3 cells, a doxycycline-inducible neuroblastoma cell model of MYCN overexpression (fig. S4, C and D). CBL0137 was highly toxic to a panel of seven human neuroblastoma cell lines compared with normal fibroblasts and was particularly potent against neuroblastoma cell lines with high c-MYC or MYCN protein expression (Fig. 4A and figs. S1N and S4E). Consistent with this observation, CBL0137 markedly decreased colony-forming capacity of doxycycline-treated SHEP.MYCN3 cells, as well as *MYCN* mRNA, MYCN protein, and MYCN binding to the promoter of FACT subunits in BE(2)C and KELLY cells (Fig. 4, B to D, and fig. S4F).

We have previously shown that CBL0137 exhibited promising antitumor efficacy in multiple preclinical cancer models (*12*), so we next examined CBL0137 in vivo against established neuroblastoma in *TH-MYCN*$^{+/+}$mice. Intravenous administration of CBL0137 (60 mg/kg;

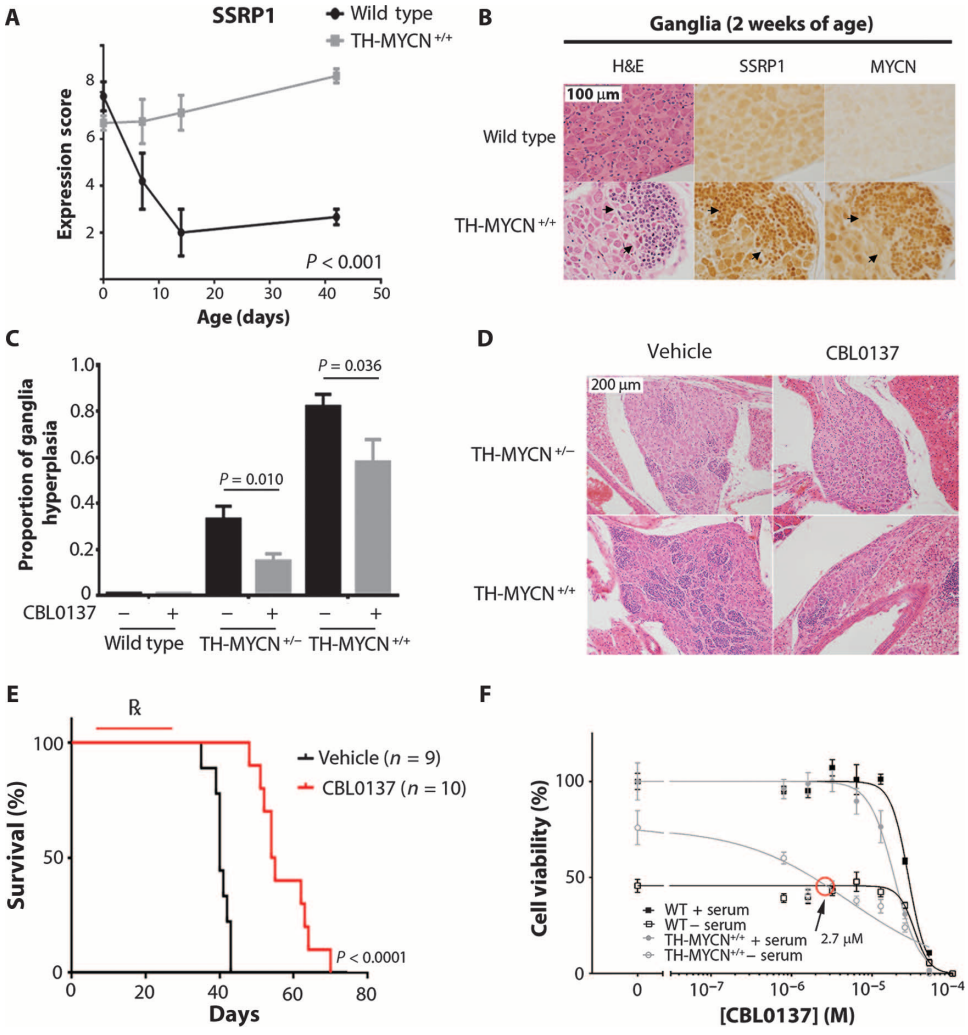

Fig. 3. CBL0137 overcomes developmental signals that drive neuroblast persistence in *TH-MYCN* mice. (**A**) Semiquantitative histology scoring was used to determine the relative expression of SSRP1 in wild-type and *TH-MYCN*$^{+/+}$ mice through perinatal time points as indicated. *P* value was calculated using analysis of variance (ANOVA), testing the significance of genotype as the source of variation. At least three independent mice had one or more ganglia present for analysis for each time point/genotype. (**B**) Representative immunohistochemistry images comparing serial ganglion sections of 2-week-old wild-type and *TH-MYCN*$^{+/+}$ mice. Hematoxylin and eosin (H&E) staining and immunoblotting for SSRP1 and MYCN are shown. Arrowheads indicate areas of neuroblast hyperplasia. (**C**) Six-day-old wild-type, *TH-MYCN*$^{+/-}$, and *TH-MYCN*$^{+/+}$ mice were treated with intraperitoneal vehicle control (0.2% methylcellulose) or CBL0137 for 5 days (10 mg/kg per day), and the proportion of ganglia with hyperplastic neuroblasts was evaluated by histological examination. Ganglia were considered to be hyperplastic if >30 focal neuroblasts were present per ganglion. Data displayed indicate the average proportion of hyperplastic ganglia per mouse ± SE. Sample sizes were as follows: wild type/vehicle, 6; wild type/CBL0137, 4; TH-MYCN$^{+/-}$/vehicle, 13; TH-MYCN$^{+/-}$/CBL0137, 13; TH-MYCN$^{+/+}$/vehicle, 9; and TH-MYCN$^{+/+}$/CBL0137, 9. (**D**) Representative H&E images of ganglion histology from mice treated as in (C). (**E**) Six-day-old *TH-MYCN*$^{+/+}$ mice were treated with intraperitoneal vehicle control (0.2% methylcellulose × 5 days/week) or CBL0137 for 3 weeks (10 mg/kg per day × 5 days/week) and thereafter assessed for tumor growth. A Kaplan-Meier plot is displayed for vehicle- or CBL0137-treated mice considering time to maximum tumor burden (when tumors were 10 mm in diameter by palpation). ℞ indicates treatment period. Log-rank test was used to calculate statistical significance between CBL0137 and vehicle-treated tumors. (**F**) Primary sympathetic ganglia were isolated and cultured from 2-week-old *TH-MYCN*$^{+/+}$ or wild-type age-matched controls. Ganglia cultures were treated with serum-rich or serum-deprived medium (1 of 30 normal concentration of serum) for 48 hours, as well as with various concentrations of CBL0137 for 24 hours, and viability was calculated by cell counts on βIII-tubulin–positive cells for each of the *TH-MYCN*$^{+/+}$ or wild-type cultures. Plot shows the nonlinear regression line of percentage cell viability as determined by counts for βIII-tubulin–positive immunofluorescence normalized to untreated/serum-rich samples for each of the *TH-MYCN*$^{+/+}$ or wild-type cultures. Data displayed represent average cell viability ± SE from the combined data of three independent biological replicates. Red circle indicates the concentration of CBL0137 that causes serum-deprived *TH-MYCN*$^{+/+}$ cultures to have equal cell viability to serum-deprived wild-type cultures.

every 4 days for eight doses) to 6-week-old *TH-MYCN*$^{+/+}$ mice with advanced neuroblastoma delayed tumor growth, with most mice exhibiting long-term tumor regression (Fig. 5A and fig. S5A). Oral CBL0137 (20 mg/kg; five doses weekly for 4 weeks) and low-dose intravenous CBL0137 (40 mg/kg; every 4 days for eight doses) were less effective but still prolonged time until maximum tumor burden (Fig. 5A and

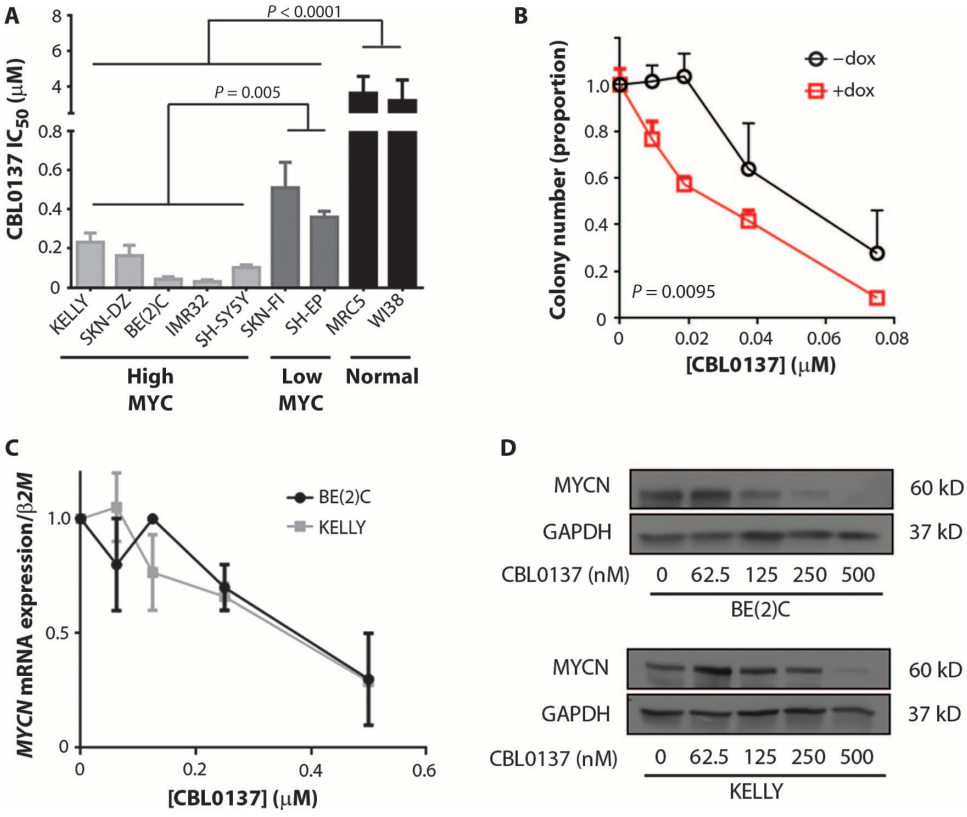

Fig. 4. High MYCN expression sensitizes neuroblastoma cells to CBL0137. (**A**) CBL0137 IC_{50} (50% inhibitory concentration) was determined from resazurin reduction assays on a panel of neuroblastoma cell lines and primary lung fibroblast controls. Cells were classified as high and low MYC-expressing cell lines on the basis of their MYCN or c-MYC expression as displayed in fig. S1N. Data displayed are 72 hours after treatment. IC_{50} was determined using nonlinear regression analysis from at least three independent biological replicates. Average IC_{50} ± SE is shown. (**B**) Colony assays were conducted for doxycycline (dox)–inducible MYCN overexpressing SHEP.MYCN3 cells (*42*) treated with an escalating dose of CBL0137. The graph shows the average number of colonies at each concentration of drug from three independent biological replicates + SE. Extra sum of squares *F* test was used to determine statistical significance between nonlinear regression of +dox (+MYCN) versus −dox (−MYCN) cells. (**C**) *MYCN* mRNA expression in BE(2)C and KELLY cells treated with increasing concentrations of CBL0137. Data are displayed as mean-normalized mRNA expression from three replicate experiments ± SE. Data obtained are 48 hours after treatment. *β2-Microglobulin* was used as a reference gene. (**D**) Western blot for MYCN protein expression in BE(2)C and KELLY cells treated with increasing concentrations of CBL0137. Data displayed are 48 hours after treatment. GAPDH was used as a loading control.

fig. S5A). We next examined the histology of tumors derived from *TH-MYCN*$^{+/+}$ mice after short-term CBL0137 treatment as either an oral (20 mg/kg for 5 days) or an intravenous (20, 40, or 60 mg/kg for 1 day) formulation. We found that the tumor tissue demonstrated a marked treatment effect, particularly for the intravenously treated (60 mg/kg) group, characterized by extensive necrosis, hemorrhage, and apoptosis compared to controls (Fig. 5B, fig. S5B, and tables S5 and S6). Moreover, intravenous CBL0137 (60 mg/kg)–treated mice exhibited evidence of metastatic regression with no mice demonstrating pulmonary metastases, whereas vehicle- and low-dose CBL0137–treated mice demonstrated marked metastatic spread to the lungs (fig. S5C). There was a substantial accumulation of CBL0137 in treated tumors compared to other organs/body fluids, with intravenous CBL0137 (60 mg/kg)–treated animals showing the highest concentrations of intratumoral CBL0137 (fig. S5D). Tumor concentrations of CBL0137 also showed a strong inverse correlation with tumor viability (Fig. 5C and fig. S5E). SSRP1, SPT16, and MYCN protein expression was decreased in intravenous CBL0137 (60 mg/kg)–treated tumors compared to both oral CBL0137 and vehicle treatment (Fig. 5D). Moreover, intravenous administration of CBL0137 to BALB/c nude mice bearing flank xenografts of the human neuroblastoma cell line BE(2)C resulted in delayed tumor growth and decreased MYCN protein expression (fig. S5, F and G). Together, this suggests that the inhibitory effect of CBL0137 on FACT has a downstream negative impact on MYCN expression and results in a marked therapeutic selectivity for MYCN-driven neuroblastoma tissues in vitro and in vivo.

CBL0137 exhibits synergy with DNA-damaging cytotoxic chemotherapy

Knockdown of SSRP1 has been previously identified to sensitize ovarian and breast cancer cells to cytotoxic chemotherapy (*22*), suggesting that CBL0137 may enhance neuroblastoma chemotherapy. We used colony formation and cell viability assays in neuroblastoma cells to demonstrate that CBL0137 synergizes with mafosfamide (the active metabolite of cyclophosphamide) and that this synergy was exclusive to neuroblastoma cells in comparison with normal primary fibroblasts (Fig. 6A and fig. S6A). The combination of CBL0137 and mafosfamide was far more toxic in neuroblastoma cells compared to normal controls, indicating that a wide therapeutic index exists for this combination treatment (fig. S6B). CBL0137 combination synergy extended to several other chemotherapeutics used in neuroblastoma therapy, albeit with some exceptions (fig. S6, C and D). Consistent with these findings, cyclophosphamide, etoposide, cisplatin, and vincristine each potently increased CBL0137 efficacy in vivo against established *TH-MYCN*$^{+/+}$ tumors (Fig. 6B). Moreover, when intravenous CBL0137 was combined with clinically relevant chemotherapy regimens used to treat high-risk/refractory neuroblastoma patients, namely, cyclophosphamide/topotecan and irinotecan/temozolomide, strong tumor delay was observed in both the *TH-MYCN*$^{+/+}$transgenic mice (Fig. 6C) and BALB/c nude mice harboring BE(2)C xenografts (fig. S6E). Combination therapies were mostly well tolerated in recipient mice, with CBL0137/vincristine a notable exception. Some occasions of weight loss were observed, and mice were removed from the study as follows: cisplatin (2 of 10 mice), cisplatin/CBL0137 (2 of 10 mice), vincristine/CBL0137 (5 of 10 mice), and CBL0137/irinotecan/temozolomide (2 of 10 mice).

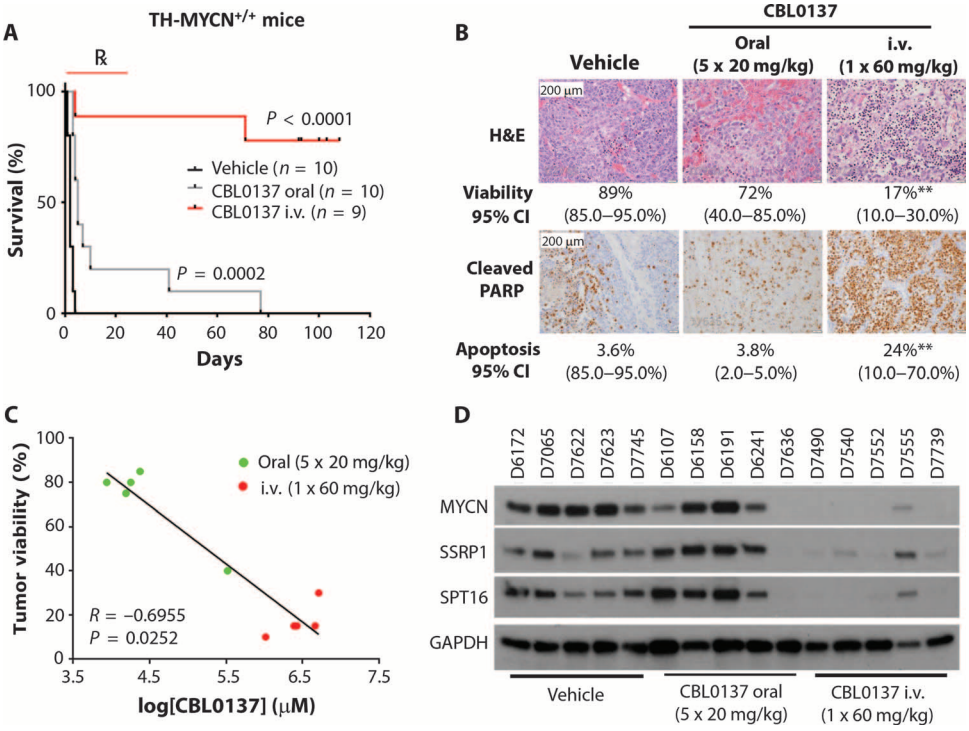

Fig. 5. CBL0137 cytotoxicity in *TH-MYCN*$^{+/+}$ tumors is associated with inhibition of the FACT/MYCN positive feedback loop. (**A**) Kaplan-Meier plot for survival of 6-week-old tumor-bearing *TH-MYCN*$^{+/+}$ mice treated with vehicle [5% dextrose given intravenously (i.v.)], oral CBL0137 (20 mg/kg; 5 days/week for 4 weeks), or intravenous CBL0137 (60 mg/kg; once every 4 days for 4 weeks). Log-rank test was used to determine statistical significance between both CBL0137-treated groups compared to vehicle. Mice began treatment when medium-sized (~5-mm-diameter) palpable tumors were detected. Endpoint was when tumors reached 10 mm by palpation. R indicates treatment period. (**B**) Representative images for H&E staining or cleaved poly(adenosine diphosphate–ribose) polymerase (cPARP) in *TH-MYCN*$^{+/+}$ tumors treated with oral CBL0137 (5 days at 20 mg/kg per day) or intravenous CBL0137 (1 day at 60 mg/kg per day). Quantitation of tumor viability or cPARP-positive cells and 95% confidence interval (95% CI) are displayed for each treatment group. Statistical significance was determined using Mann-Whitney test. $^{**}P < 0.01$. See table S7 for individual *P* values. (**C**) Correlation of CBL0137 tissue concentration and tumor viability in CBL0137-treated tumors treated as in (B). *P* and *R* values were determined using Spearman's rank correlation coefficient. (**D**) Western blot for MYCN, SSRP1, and SPT16 protein expression in individual *TH-MYCN*$^{+/+}$ tumors treated as in (B). GAPDH was used as a loading control. Tumor identifiers are indicated above each lane.

DISCUSSION

Pathologic epigenetic regulation of transcription by abnormal chemical modification of histone tails and DNA methylation has been extensively studied in human cancer (*25*). However, less is known about the role of nucleosome remodelers, such as the histone chaperone proteins in cancer (*26*). Here, we used a MYC target gene expression signature to identify the H2A/H2B histone chaperone FACT as a key driver and treatment target in the MYCN-driven pediatric cancer neuroblastoma. FACT and MYCN expression acted in a forward feedback loop, and chemical inhibition of FACT impaired neuroblastoma initiation, suggesting that FACT and MYCN may together inhibit developmentally timed maturation signals in *TH-MYCN*$^{+/+}$ mice. This oncogenic cooperation between MYCN and FACT created a synthetic lethality when conventional DNA-damaging chemotherapy was administered with the FACT inhibitor CBL0137, providing the mechanistic basis for a combination anticancer therapy approach.

Aberrant activity of nucleosome remodeling proteins has been observed in pediatric cancer. Most evidence suggests that these proteins more frequently act as tumor suppressors, as evidenced by the loss-of-function mutations in *SWI/SNF* complexes in malignant rhabdoid tumors (*27*) and genomic alterations of the H3.3 chaperone *ATRX* in neuroblastoma (*14*) and pediatric glioma (*28*). In contrast, our data support a gain-of-function model whereby FACT is present in pathologically high amounts in cancer tissues. Although there are other examples of similar "oncogenic" histone chaperones such as DEK (*29*) and CHAF1A (*30*), this study identifies an oncogenic histone chaperone that has a potent and effective chemical inhibitor available for clinical use.

FACT is normally expressed in embryonal or primitive tissues and is thereafter down-regulated during tissue differentiation and in mature tissues, in a manner similar to MYCN (*11*, *13*, *31*). We showed a strong correlation between MYCN and FACT expression in normal sympathetic ganglia, including high expression in normal developmental neuroblasts, the putative cell of origin of neuroblastoma (*15*, *18*). *SSRP1* knockout mice are embryonic lethal before E5.5 (*32*), so later developmental roles are unknown, but this expression pattern suggests that FACT may function in physiological regulation of sympathoadrenal development. Our data show that FACT expression is also correlated with MYCN at tumor initiation, and chemical inhibition of FACT delayed neuroblastoma onset. This suggests that FACT may have functions in neuroblastoma tumor initiation and progression. This is consistent with the observation that aberrant expression or activity of developmental

FACT was previously implicated in cisplatin resistance as part of a DNA repair complex containing DNA-PK (DNA-dependent protein kinase) (*22*), and it is well established to have roles in DNA repair (*8*, *23*, *24*). Thus, we reasoned that the synergy exhibited by CBL0137 in combination with genotoxic chemotherapy may be dependent on inhibiting FACT during DNA repair. Thus, we next examined the extent of DNA repair when CBL0137 was added to cells after they were treated with the genotoxic agents cisplatin or etoposide. CBL0137 inhibited DNA double-strand break repair, which otherwise occurred after withdrawal of either cisplatin or etoposide, even though CBL0137 exhibited no genotoxicity alone (Fig. 7A). Moreover, CBL0137 resulted in a marked increase in DNA damage markers γH2AX and 53BP1 in the presence of etoposide (Fig. 7, B and C). These findings were recapitulated when inhibition of DNA repair by CBL0137 was evaluated after hydroxyurea treatment, but not when CBL0137 was added after vincristine (fig. S7, A and B), suggesting that the synergistic action of CBL0137 was specific to direct DNA-damaging agents and not microtubule poisons.

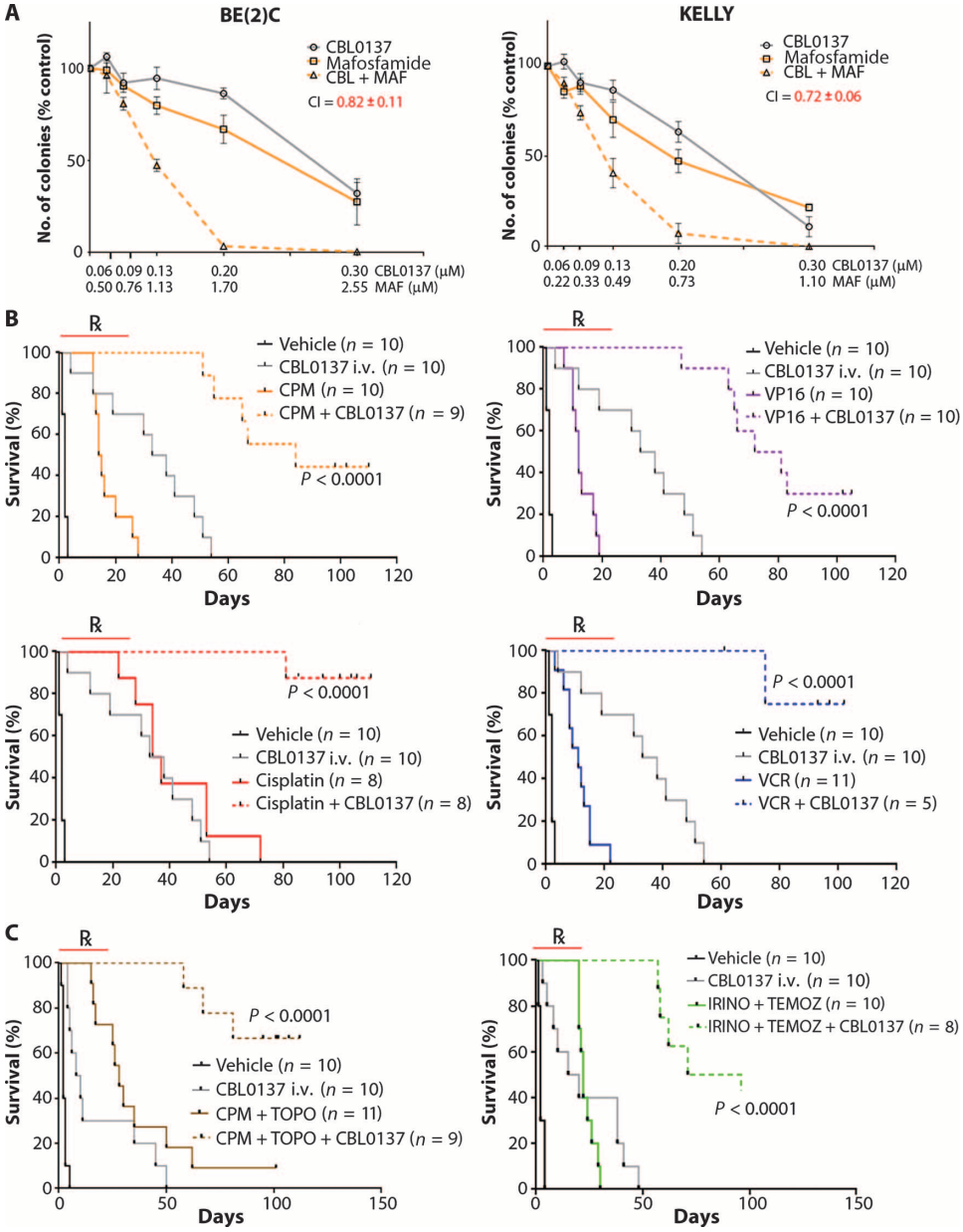

Fig. 6. CBL0137 synergizes with neuroblastoma chemotherapy. (**A**) Colony-forming assays were performed for BE(2)C and KELLY cells treated with CBL0137 (CBL) in combination with mafosfamide (MAF), the active metabolite of cyclophosphamide. Combination index (CI) at a fractional cell kill of 0.80 is shown using the Chou-Talalay method (*43*). CI <0.9, synergistic. Data are displayed as the average number of colonies at each concentration of drugs from three independent biological replicates ± SE. (**B**) Kaplan-Meier plots of tumor-bearing *TH-MYCN*$^{+/+}$ mice treated with vehicle (5% dextrose) or intravenous CBL0137 (40 mg/kg; once every 4 days for 4 weeks) combined with cyclophosphamide (CPM; 15 mg/kg per day), etoposide (VP16; 6 mg/kg per day), cisplatin (2 mg/kg per day), or vincristine (VCR; 2 mg/kg per day). Mice were treated starting at 6 weeks of age, when 5-mm palpable tumors were detected. Endpoint was at 10-mm tumor diameter by palpation. Cyclophosphamide, etoposide, cisplatin, and vincristine were all administered intraperitoneally for five consecutive days when treatment began. *P* value was determined using pairwise log-rank test for CBL0137/chemotherapy combinations versus their respective single treatment controls. ℞ indicates treatment period. (**C**) Kaplan-Meier plots of tumor-bearing *TH-MYCN*$^{+/+}$ mice treated with vehicle (5% dextrose) or intravenous CBL0137 (40 mg/kg; once every 4 days for 4 weeks) combined with cyclophosphamide (10 mg/kg per day) and topotecan (TOPO; 5 mg/kg per day) (left) or irinotecan (IRINO; 2 mg/kg per day) and temozolomide (TEMOZ; 5 mg/kg per day) (right). Mice were treated at 6 weeks of age, starting when 5-mm palpable tumors were detected. Endpoint was at 10-mm tumor diameter by palpation. Cyclophosphamide, topotecan, irinotecan, and temozolomide were all administered intraperitoneally for five consecutive days when treatment began. *P* value was determined using pairwise log-rank test for CBL0137/chemotherapy combinations versus their respective treatment controls. ℞ indicates treatment period.

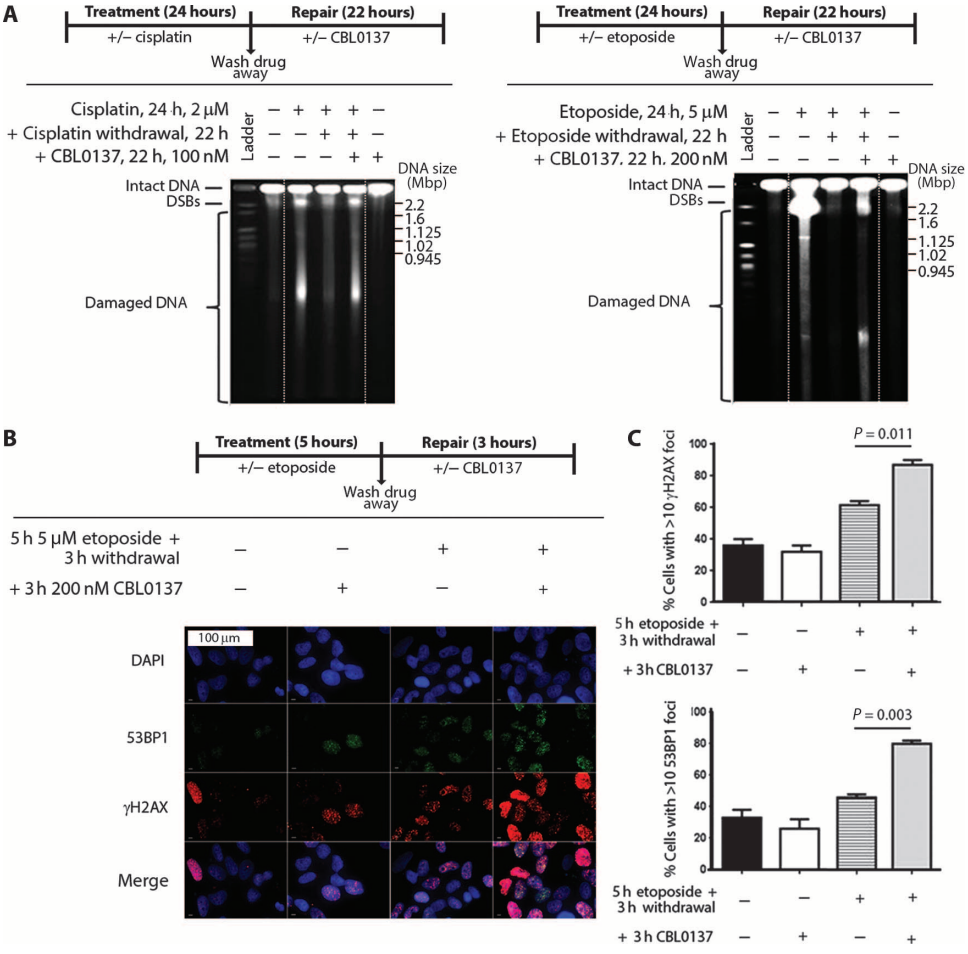

Fig. 7. CBL0137 prevents DNA damage repair after genotoxic chemotherapy. (**A**) BE(2)C cells were treated for 24 hours with or without the following chemotherapeutics: 2 μM cisplatin (left) or 5 μM etoposide (right). Chemotherapeutics were subsequently removed, and medium was supplemented with or without 100 nM CBL0137 for 22 hours (refer to schematic above gel for the administration schedule). The repair of chemotherapy-induced DNA double-strand breaks (DSBs) in the presence or absence of CBL0137 was determined using pulsed-field gel electrophoresis. Data displayed are representative of two independent biological replicates. Dashed white lines indicate areas where gel was cropped for presentation. (**B**) BE(2)C cells were treated with or without 5 μM etoposide for 5 hours. Etoposide was subsequently removed, and medium was supplemented with or without 200 nM CBL0137 for 3 hours (refer to schematic above the images for the administration schedule). Cells were then fixed and processed for immunofluorescence with anti-γH2AX (red) and anti-53BP1 (green), as well as 4′,6-diamidino-2-phenylindole (DAPI) DNA stain (blue). (**C**) From (B), quantitation of the percentage of cells with >10 positive immunofluorescent foci for DNA damage markers γH2AX (top) or 53BP1 (bottom). Data are displayed as the average percentage of positive cells ± SE from two independent biological replicates. Mbp, mega base pairs.

regulators are key determinants of neuroblastoma tumorigenesis (*18*). Animal models with conditional knockout of *SSRP1* or *SPT16* will reveal more specific roles of FACT in sympathoadrenal development and, by association, in MYCN-driven tumorigenesis.

FACT controls nucleosome "eviction" and "reassembly" of histones, thus promoting the smooth passage of RNA polymerase II during gene transcription (*8*, *9*, *33*). Our previous data have demonstrated that SSRP1 is enriched at the promoter regions of oncogene transcription factors and their respective transcriptional targets (*10*). We show here that FACT maintains high concentrations of MYCN protein in neuroblastoma cells by driving MYCN transcription and protein stability. Moreover, FACT is a functional cofactor to oncogenic mutant H-Ras^{V12} in malignant transformation of mammary epithelial cells (*10*). These observations support a model whereby FACT drives both malignant transcription and oncogenic transcription factor activity, yet the mechanism that governs FACT transcriptional specificity in cancer cells remains unclear. It may simply be that inappropriate expression of FACT in normal cell types is sufficient to collaborate with other oncogenic transcription factors to drive a gene program that favors malignant transformation and transcription.

Our results demonstrate that FACT can enhance MYCN transcription and protein stability in neuroblastoma cells, even those with multiple copies of *MYCN* and an already high MYCN expression. Although *MYCN* amplification is a common feature of human neuroblastoma, recent studies have indicated that mechanisms in addition to gene amplification are required to maintain the very high MYCN protein concentrations necessary for the fully malignant phenotype (*34*–*37*). Collectively, these findings are consistent with observations made in tumorigenic murine *Myc* models showing that different thresholds of MYC expression result in different components of the malignant phenotype, and suggest that MYCN expression and protein stability are important treatment targets (*38*).

For neuroblastoma patients with advanced disease, prognosis is still poor (*1*, *2*). Many of these patients' tumors are characterized by *MYCN* amplification or overactivation of MYC target genes (*6*). We show here that CBL0137 was highly effective against established primary tumors and pulmonary metastases in *TH-MYCN*$^{+/+}$ mice and that CBL0137 treatment was accompanied by marked MYCN depletion in tumors after only a single intravenous dose, suggesting that targeting FACT may be an important strategy to decrease MYCN expression and overcome primary and metastatic disease (*37*, *39*–*41*). This treatment approach is particularly promising because the expression of MYCN and FACT is markedly higher in malignant compared with normal tissues (*10*, *11*, *15*). Accordingly, our data showed that CBL0137 inhibition of FACT and MYCN was associated with extensive cytotoxicity in advanced *TH-MYCN*$^{+/+}$ tumors but exhibited minimal toxicity, consistent with findings in other animal models of cancer (*12*). Moreover, the previously described inhibitory activity of CBL0137 against nuclear factor κB (NFκB)transcriptional targeting and activation of p53 by casein kinase–dependent Ser^{32} phosphorylation (*12*) makes CBL0137 a potential multimodal cancer therapeutic

for a variety of malignancies characterized by defects within these pathways.

FACT has been shown to promote DNA damage repair in the face of DNA-damaging chemotherapy (*22*), suggesting that it may act as a chemoresistance factor. Here, we showed that CBL0137 was particularly effective as a combination therapy with chemotherapeutic agents. In addition, combining CBL0137 with chemotherapy regimens currently used after relapse potentiated its activity, highlighting a potential therapeutic strategy for high-risk neuroblastoma patients. Although our data and those of others have shown that CBL0137 alone is not genotoxic (*12*), inhibition of FACT created a synthetic lethal environment in the presence of cisplatin and etoposide but not vincristine. Moreover, combinations of CBL0137 with DNA-damaging agents such as cisplatin, cyclophosphamide, and etoposide were better tolerated in our mouse models than the nongenotoxic microtubule inhibitor vincristine, suggesting that the most effective role for CBL0137 in anticancer therapy will be coadministration with primary DNA-damaging agents. We also observed that p53 status was not a determinant of CBL0137 combination therapy sensitivity, consistent with previous findings for CBL0137 as a single agent in adult cancer types (*12*). Considering that genotoxic chemotherapy is associated with marked nonspecific toxicity in patients, targeting FACT with the nongenotoxic CBL0137 promises to enhance cancer cell specificity of these agents, which are the current mainstay of neuroblastoma therapy.

Future studies will need to address some of the limitations of this study. First, it will be necessary to unveil the specific mechanism by which FACT modifies MYCN expression at both the transcriptional and posttranslational level. Second, we still lack in-depth understanding of the mechanism and consequences of CBL0137-induced changes in chromatin, in particular how this relates to inhibition of FACT-dependent transcriptional programs and to specific DNA repair pathways that are affected. Detailed analyses of CBL0137 effects on DNA repair pathways such as homologous repair and nonhomologous end joining will be required. Third, the mechanism by which CBL0137 accumulates at high concentration in neuroblastoma tumors and whether this occurs in other cancer types are unknown. In particular, mechanisms of CBL0137 uptake, metabolism, and efflux will need to be elucidated. Finally, it remains to be explored whether CBL0137 can be used as a therapy for other cancers and whether MYC deregulation can serve as a biomarker for CBL0137 sensitivity. With these additional studies, CBL0137 or newer FACT inhibitors may serve as a therapy for neuroblastoma and potentially other MYC-driven cancers.

MATERIALS AND METHODS

Detailed methods are available in the Supplementary Materials.

SUPPLEMENTARY MATERIALS

www.sciencetranslationalmedicine.org/cgi/content/full/7/312/312ra176/DC1
Materials and Methods
Fig. S1. Data supporting Fig. 1.
Fig. S2. Data supporting Fig. 2.
Fig. S3. Data supporting Fig. 3.
Fig. S4. Data supporting Fig. 4.
Fig. S5. Data supporting Fig. 5.
Fig. S6. Data supporting Fig. 6.
Fig. S7. Data supporting Fig. 7.
Fig. S8. Fluorescence in situ hybridization for MYCN amplification in tissue microarray.
Table S1. Cox proportional hazards modeling of MYC target signature members in 649 neuroblastoma patients.
Table S2. Literature analysis of lead candidates that favor poor outcome in neuroblastoma.
Table S3. Cox proportional hazards modeling of SSRP1 and SPT16 in 649 neuroblastoma patients.
Table S4. Gene set enrichment analysis of 2-week-old *TH-MYCN*$^{+/+}$ ganglia compared with age-matched wild-type mice.
Table S5. Histology of *TH-MYCN*$^{+/+}$ mice treated with oral or intravenous CBL0137.
Table S6. Histology of *TH-MYCN*$^{+/+}$ mice treated with a dose-escalating regimen of intravenous CBL0137.
Table S7. *P* values not shown in figures.
References (*44*–*59*)

REFERENCES AND NOTES

1. G. M. Brodeur, Neuroblastoma: Biological insights into a clinical enigma. *Nat. Rev. Cancer* **3**, 203–216 (2003).
2. J. M. Maris, Recent advances in neuroblastoma. *N. Engl. J. Med.* **362**, 2202–2211 (2010).
3. M. Schwab, K. Alitalo, K.-H. Klempnauer, H. E. Varmus, J. M. Bishop, F. Gilbert, G. Brodeur, M. Goldstein, J. Trent, Amplified DNA with limited homology to *myc* cellular oncogene is shared by human neuroblastoma cell lines and a neuroblastoma tumour. *Nature* **305**, 245–248 (1983).
4. H. Kocak, S. Ackermann, B. Hero, Y. Kahlert, A. Oberthuer, D. Juraeva, F. Roels, J. Theissen, F. Westermann, H. Deubzer, V. Ehemann, B. Brors, M. Odenthal, F. Berthold, M. Fischer, Hox-C9 activates the intrinsic pathway of apoptosis and is associated with spontaneous regression in neuroblastoma. *Cell Death Dis.* **4**, e586 (2013).
5. W. A. Weiss, K. Aldape, G. Mohapatra, B. G. Feuerstein, J. M. Bishop, Targeted expression of *MYCN* causes neuroblastoma in transgenic mice. *EMBO J.* **16**, 2985–2995 (1997).
6. F. Westermann, D. Muth, A. Benner, T. Bauer, K.-O. Henrich, A. Oberthuer, B. Brors, T. Beissbarth, J. Vandesompele, F. Pattyn, B. Hero, R. König, M. Fischer, M. Schwab, Distinct transcriptional MYCN/c-MYC activities are associated with spontaneous regression or malignant progression in neuroblastomas. *Genome Biol.* **9**, R150 (2008).
7. H. Ji, G. Wu, X. Zhan, A. Nolan, C. Koh, A. De Marzo, H. M. Doan, J. Fan, C. Cheadle, M. Fallahi, J. L. Cleveland, C. V. Dang, K. I. Zeller, Cell-type independent MYC target genes reveal a primordial signature involved in biomass accumulation. *PLOS One* **6**, e26057 (2011).
8. T. Formosa, The role of FACT in making and breaking nucleosomes. *Biochim. Biophys. Acta* **1819**, 247–255 (2012).
9. D. Reinberg, R. J. Sims III, de FACTo nucleosome dynamics. *J. Biol. Chem.* **281**, 23297–23301 (2006).
10. H. Garcia, J. C. Miecznikowski, A. Safina, M. Commane, A. Ruusulehto, S. Kilpinen, R. W. Leach, K. Attwood, Y. Li, S. Degan, A. R. Omilian, O. Guryanova, O. Papantonopoulou, J. Wang, M. Buck, S. Liu, C. Morrison, K. V. Gurova, Facilitates chromatin transcription complex is an "accelerator" of tumor transformation and potential marker and target of aggressive cancers. *Cell Rep.* **4**, 159–173 (2013).
11. H. Garcia, D. Fleyshman, K. Kolesnikova, A. Safina, M. Commane, G. Paszkiewicz, A. Omelian, C. Morrison, K. Gurova, Expression of FACT in mammalian tissues suggests its role in maintaining of undifferentiated state of cells. *Oncotarget* **2**, 783–796 (2011).
12. A. V. Gasparian, C. A. Burkhart, A. A. Purmal, L. Brodsky, M. Pal, M. Saranadasa, D. A. Bosykh, M. Commane, O. A. Guryanova, S. Pal, A. Safina, S. Sviridov, I. E. Koman, J. Veith, A. A. Komar, A. V. Gudkov, K. V. Gurova, Curaxins: Anticancer compounds that simultaneously suppress NF-κB and activate p53 by targeting FACT. *Sci. Transl. Med.* **3**, 95ra74 (2011).
13. A. Safina, H. Garcia, M. Commane, O. Guryanova, S. Degan, K. Kolesnikova, K. V. Gurova, Complex mutual regulation of facilitates chromatin transcription (FACT) subunits on both mRNA and protein levels in human cells. *Cell Cycle* **12**, 2423–2434 (2013).
14. J. J. Molenaar, J. Koster, D. A. Zwijnenburg, P. van Sluis, L. J. Valentijn, I. van der Ploeg, M. Hamdi, J. van Nes, B. A. Westerman, J. van Arkel, M. E. Ebus, F. Haneveld, A. Lakeman, L. Schild, P. Molenaar, P. Stroeken, M. M. van Noesel, I. Øra, E. E. Santo, H. N. Caron, E. M. Westerhout, R. Versteeg, Sequencing of neuroblastoma identifies chromothripsis and defects in neuritogenesis genes. *Nature* **483**, 589–593 (2012).
15. L. M. Hansford, W. D. Thomas, J. M. Keating, C. A. Burkhart, A. E. Peaston, M. D. Norris, M. Haber, P. J. Armati, W. A. Weiss, G. M. Marshall, Mechanisms of embryonal tumor initiation: Distinct roles for MycN expression and *MYCN* amplification. *Proc. Natl. Acad. Sci. U.S.A.* **101**, 12664–12669 (2004).
16. Y. Nishida, N. Adati, R. Ozawa, A. Maeda, Y. Sakaki, T. Takeda, Identification and classification of genes regulated by phosphatidylinositol 3-kinase- and TRKB-mediated signalling pathways during neuronal differentiation in two subtypes of the human neuroblastoma cell line SH-SY5Y. *BMC Res. Notes* **1**, 95 (2008).
17. G. M. Marshall, J. L. Bell, J. Koach, O. Tan, P. Kim, A. Malyukova, W. Thomas, E. O. Sekyere, T. Liu, A. M. Cunningham, V. Tobias, M. D. Norris, M. Haber, M. Kavallaris, B. B. Cheung,

TRIM16 acts as a tumour suppressor by inhibitory effects on cytoplasmic vimentin and nuclear E2F1 in neuroblastoma cells. *Oncogene* **29**, 6172–6183 (2010).
18. G. M. Marshall, D. R. Carter, B. B. Cheung, T. Liu, M. K. Mateos, J. G. Meyerowitz, W. A. Weiss, The prenatal origins of cancer. *Nat. Rev. Cancer* **14**, 277–289 (2014).
19. M. Calao, E. O. Sekyere, H. J. Cui, B. B. Cheung, W. D. Thomas, J. Keating, J. B. Chen, A. Raif, K. Jankowski, N. P. Davies, M. V. Bekkum, B. Chen, O. Tan, T. Ellis, M. D. Norris, M. Haber, E. S. Kim, J. M. Shohet, T. N. Trahair, T. Liu, B. J. Wainwright, H. F. Ding, G. M. Marshall, Direct effects of Bmi1 on p53 protein stability inactivates oncoprotein stress responses in embryonal cancer precursor cells at tumor initiation. *Oncogene* **32**, 3616–3626 (2013).
20. P. G. Komarov, E. A. Komarova, R. V. Kondratov, K. Christov-Tselkov, J. S. Coon, M. V. Chernov, A. V. Gudkov, A chemical inhibitor of p53 that protects mice from the side effects of cancer therapy. *Science* **285**, 1733–1737 (1999).
21. L. T. Vassilev, B. T. Vu, B. Graves, D. Carvajal, F. Podlaski, Z. Filipovic, N. Kong, U. Kammlott, C. Lukacs, C. Klein, N. Fotouhi, E. A. Liu, In vivo activation of the p53 pathway by small-molecule antagonists of MDM2. *Science* **303**, 844–848 (2004).
22. J. Sand-Dejmek, G. Adelmant, B. Sobhian, A. S. Calkins, J. Marto, D. J. Iglehart, J.-B. Lazaro, Concordant and opposite roles of DNA-PK and the "facilitator of chromatin transcription" (FACT) in DNA repair, apoptosis and necrosis after cisplatin. *Mol. Cancer* **10**, 74 (2011).
23. V. Kari, A. Shchebet, H. Neumann, S. A. Johnsen, The H2B ubiquitin ligase RNF40 cooperates with SUPT16H to induce dynamic changes in chromatin structure during DNA double-strand break repair. *Cell Cycle* **10**, 3495–3504 (2011).
24. D. M. Keller, X. Zeng, Y. Wang, Q. H. Zhang, M. Kapoor, H. Shu, R. Goodman, G. Lozano, Y. Zhao, H. Lu, A DNA damage–induced p53 serine 392 kinase complex contains CK2, hSpt16, and SSRP1. *Mol. Cell* **7**, 283–292 (2001).
25. S. B. Baylin, P. A. Jones, A decade of exploring the cancer epigenome—Biological and translational implications. *Nat. Rev. Cancer* **11**, 726–734 (2011).
26. R. J. Burgess, Z. Zhang, Histone chaperones in nucleosome assembly and human disease. *Nat. Struct. Mol. Biol.* **20**, 14–22 (2013).
27. B. G. Wilson, C. W. Roberts, SWI/SNF nucleosome remodellers and cancer. *Nat. Rev. Cancer* **11**, 481–492 (2011).
28. J. Schwartzentruber, A. Korshunov, X.-Y. Liu, D. T. W. Jones, E. Pfaff, K. Jacob, D. Sturm, A. M. Fontebasso, D.-A. Quang, M. Tönjes, V. Hovestadt, S. Albrecht, M. Kool, A. Nantel, C. Konermann, A. Lindroth, N. Jäger, T. Rausch, M. Ryzhova, J. O. Korbel, T. Hielscher, P. Hauser, M. Garami, A. Klekner, L. Bognar, M. Ebinger, M. U. Schuhmann, W. Scheurlen, A. Pekrun, M. C. Frühwald, W. Roggendorf, C. Kramm, M. Dürken, J. Atkinson, P. Lepage, A. Montpetit, M. Zakrzewska, K. Zakrzewski, P. P. Liberski, Z. Dong, P. Siegel, A. E. Kulozik, M. Zapatka, A. Guha, D. Malkin, J. Felsberg, G. Reifenberger, A. von Deimling, K. Ichimura, V. P. Collins, H. Witt, T. Milde, O. Witt, C. Zhang, P. Castelo-Branco, P. Lichter, D. Faury, U. Tabori, C. Plass, J. Majewski, S. M. Pfister, N. Jabado, Driver mutations in histone H3.3 and chromatin remodelling genes in paediatric glioblastoma. *Nature* **482**, 226–231 (2012).
29. T. M. Wise-Draper, R. A. Mintz-Cole, T. A. Morris, D. S. Simpson, K. A. Wikenheiser-Brokamp, M. A. Currier, T. P. Cripe, G. C. Grosveld, S. I. Wells, Overexpression of the cellular DEK protein promotes epithelial transformation in vitro and in vivo. *Cancer Res.* **69**, 1792–1799 (2009).
30. E. Barbieri, K. De Preter, M. Capasso, Z. Chen, D. M. Hsu, G. P. Tonini, S. Lefever, J. Hicks, R. Versteeg, A. Pession, F. Speleman, E. S. Kim, J. M. Shohet, Histone chaperone CHAF1A inhibits differentiation and promotes aggressive neuroblastoma. *Cancer Res.* **74**, 765–774 (2014).
31. K. A. Zimmerman, G. D. Yancopoulos, R. G. Collum, R. K. Smith, N. E. Kohl, K. A. Denis, M. M. Nau, O. N. Witte, D. Toran-Allerand, C. E. Gee, J. D. Minna, F. W. Alt, Differential expression of *myc* family genes during murine development. *Nature* **319**, 780–783 (1986).
32. S. Cao, H. Bendall, G. G. Hicks, A. Nashabi, H. Sakano, Y. Shinkai, M. Gariglio, E. M. Oltz, H. E. Ruley, The high-mobility-group box protein SSRP1/T160 is essential for cell viability in day 3.5 mouse embryos. *Mol. Cell. Biol.* **23**, 5301–5307 (2003).
33. G. Orphanides, G. LeRoy, C.-H. Chang, D. S. Luse, D. Reinberg, FACT, a factor that facilitates transcript elongation through nucleosomes. *Cell* **92**, 105–116 (1998).
34. G. M. Marshall, P. Y. Liu, S. Gherardi, C. J. Scarlett, A. Bedalov, N. Xu, N. Iraci, E. Valli, D. Ling, W. Thomas, M. van Bekkum, E. Sekyere, K. Jankowski, T. Trahair, K. L. Mackenzie, M. Haber, M. D. Norris, A. V. Biankin, G. Perini, T. Liu, SIRT1 promotes N-Myc oncogenesis through a positive feedback loop involving the effects of MKP3 and ERK on N-Myc protein stability. *PLOS Genet.* **7**, e1002135 (2011).
35. P. Y. Liu, N. Xu, A. Malyukova, C. J. Scarlett, Y. T. Sun, X. D. Zhang, D. Ling, S.-P. Su, C. Nelson, D. K. Chang, J. Koach, A. E. Tee, M. Haber, M. D. Norris, C. Toon, I. Rooman, C. Xue, B. B. Cheung, S. Kumar, G. M. Marshall, A. V. Biankin, T. Liu, The histone deacetylase SIRT2 stabilizes Myc oncoproteins. *Cell Death Differ.* **20**, 503–514 (2013).
36. T. Otto, S. Horn, M. Brockmann, U. Eilers, L. Schüttrumpf, N. Popov, A. M. Kenney, J. H. Schulte, R. Beijersbergen, H. Christiansen, B. Berwanger, M. Eilers, Stabilization of N-Myc is a critical function of Aurora A in human neuroblastoma. *Cancer Cell* **15**, 67–78 (2009).
37. L. Chesler, C. Schlieve, D. D. Goldenberg, A. Kenney, G. Kim, A. McMillan, K. K. Matthay, D. Rowitch, W. A. Weiss, Inhibition of phosphatidylinositol 3-kinase destabilizes Mycn protein and blocks malignant progression in neuroblastoma. *Cancer Res.* **66**, 8139–8146 (2006).
38. D. J. Murphy, M. R. Junttila, L. Pouyet, A. Karnezis, K. Shchors, D. A. Bui, L. Brown-Swigart, L. Johnson, G. I. Evan, Distinct thresholds govern Myc's biological output in vivo. *Cancer Cell* **14**, 447–457 (2008).
39. Y. H. Chanthery, W. C. Gustafson, M. Itsara, A. Persson, C. S. Hackett, M. Grimmer, E. Charron, S. Yakovenko, G. Kim, K. K. Matthay, W. A. Weiss, Paracrine signaling through MYCN enhances tumor-vascular interactions in neuroblastoma. *Sci. Transl. Med.* **4**, 115ra113 (2012).
40. J. E. Delmore, G. C. Issa, M. E. Lemieux, P. B. Rahl, J. Shi, H. M. Jacobs, E. Kastritis, T. Gilpatrick, R. M. Paranal, J. Qi, M. Chesi, A. C. Schinzel, M. R. McKeown, T. P. Heffernan, C. R. Vakoc, P. L. Bergsagel, I. M. Ghobrial, P. G. Richardson, R. A. Young, W. C. Hahn, K. C. Anderson, A. L. Kung, J. E. Bradner, C. S. Mitsiades, BET bromodomain inhibition as a therapeutic strategy to target c-Myc. *Cell* **146**, 904–917 (2011).
41. A. Puissant, S. M. Frumm, G. Alexe, C. F. Bassil, J. Qi, Y. H. Chanthery, E. A. Nekritz, R. Zeid, W. C. Gustafson, P. Greninger, M. J. Garnett, U. McDermott, C. H. Benes, A. L. Kung, W. A. Weiss, J. E. Bradner, K. Stegmaier, Targeting MYCN in neuroblastoma by BET bromodomain inhibition. *Cancer Discov.* **3**, 308–323 (2013).
42. A. Slack, Z. Chen, R. Tonelli, M. Pule, L. Hunt, A. Pession, J. M. Shohet, The p53 regulatory gene *MDM2* is a direct transcriptional target of MYCN in neuroblastoma. *Proc. Natl. Acad. Sci. U.S.A.* **102**, 731–736 (2005).
43. T. C. Chou, P. Talalay, Quantitative analysis of dose-effect relationships: The combined effects of multiple drugs or enzyme inhibitors. *Adv. Enzyme Regul.* **22**, 27–55 (1984).
44. L. Chesler, W. A. Weiss, Genetically engineered murine models—Contribution to our understanding of the genetics, molecular pathology and therapeutic targeting of neuroblastoma. *Semin. Cancer Biol.* **21**, 245–255 (2011).
45. M. E. H. Hammond, D. F. Hayes, M. Dowsett, D. C. Allred, K. L. Hagerty, S. Badve, P. L. Fitzgibbons, G. Francis, N. S. Goldstein, M. Hayes, D. G. Hicks, S. Lester, R. Love, P. B. Mangu, L. McShane, K. Miller, C. K. Osborne, S. Paik, J. Perlmutter, A. Rhodes, H. Sasano, J. N. Schwartz, F. C. G. Sweep, S. Taube, E. E. Torlakovic, P. Valenstein, G. Viale, D. Visscher, T. Wheeler, R. B. Williams, J. L. Wittliff, A. C. Wolff, American Society of Clinical Oncology/College of American Pathologists guideline recommendations for immunohistochemical testing of estrogen and progesterone receptors in breast cancer. *J. Clin. Oncol.* **28**, 2784–2795 (2010).
46. V. K. Mootha, C. M. Lindgren, K.-F. Eriksson, A. Subramanian, S. Sihag, J. Lehar, P. Puigserver, E. Carlsson, M. Ridderstråle, E. Laurila, N. Houstis, M. J. Daly, N. Patterson, J. P. Mesirov, T. R. Golub, P. Tamayo, B. Spiegelman, E. S. Lander, J. N. Hirschhorn, D. Altshuler, L. C. Groop, PGC-1α-responsive genes involved in oxidative phosphorylation are coordinately downregulated in human diabetes. *Nat. Genet.* **34**, 267–273 (2003).
47. A. Subramanian, P. Tamayo, V. K. Mootha, S. Mukherjee, B. L. Ebert, M. A. Gillette, A. Paulovich, S. L. Pomeroy, T. R. Golub, E. S. Lander, J. P. Mesirov, Gene set enrichment analysis: A knowledge-based approach for interpreting genome-wide expression profiles. *Proc. Natl. Acad. Sci. U.S.A.* **102**, 15545–15550 (2005).
48. C. A. Burkhart, A. J. Cheng, J. Madafiglio, M. Kavallaris, M. Mili, G. M. Marshall, W. A. Weiss, L. M. Khachigian, M. D. Norris, M. Haber, Effects of MYCN antisense oligonucleotide administration on tumorigenesis in a murine model of neuroblastoma. *J. Natl. Cancer Inst.* **95**, 1394–1403 (2003).
49. M. J. Henderson, M. Haber, A. Porro, M. A. Munoz, N. Iraci, C. Xue, J. Murray, C. L. Flemming, J. Smith, J. I. Fletcher, S. Gherardi, C.-K. Kwek, A. J. Russell, E. Valli, W. B. London, A. B. Buxton, L. J. Ashton, A. C. Sartorelli, S. L. Cohn, M. Schwab, G. M. Marshall, G. Perini, M. D. Norris, ABCC multidrug transporters in childhood neuroblastoma: Clinical and biological effects independent of cytotoxic drug efflux. *J. Natl. Cancer Inst.* **103**, 1236–1251 (2011).
50. H. Shimada, I. M. Ambros, L. P. Dehner, J.-i. Hata, V. V. Joshi, B. Roald, Terminology and morphologic criteria of neuroblastic tumors: Recommendations by the International Neuroblastoma Pathology Committee. *Cancer* **86**, 349–363 (1999).
51. H. Shimada, I. M. Ambros, L. P. Dehner, J.-i. Hata, V. V. Joshi, B. Roald, D. O. Stram, R. B. Gerbing, J. N. Lukens, K. K. Matthay, R. P. Castleberry, The International Neuroblastoma Pathology Classification (the Shimada system). *Cancer* **86**, 364–372 (1999).
52. R. I. Geran, N. H. Greenberg, M. M. Macdonald, A. M. Schumacher, B. J. Abbott, Protocols for screening chemical agents and natural products against animal tumors and other biological systems. *Cancer Chemother. Rep.* **3**, 51–61 (1972).
53. T.-C. Chou, Drug combination studies and their synergy quantification using the Chou-Talalay method. *Cancer Res.* **70**, 440–446 (2010).
54. N. Issaeva, H. D. Thomas, T. Djureinovic, J. E. Jaspers, I. Stoimenov, S. Kyle, N. Pedley, P. Gottipati, R. Zur, K. Sleeth, V. Chatzakos, E. A. Mulligan, C. Lundin, E. Gubanova, A. Kersbergen, A. L. Harris, R. A. Sharma, S. Rottenberg, N. J. Curtin, T. Helleday, 6-Thioguanine selectively kills BRCA2-defective tumors and overcomes PARP inhibitor resistance. *Cancer Res.* **70**, 6268–6276 (2010).
55. V. Marcel, S. E. Ghayad, S. Belin, G. Therizols, A.-P. Morel, E. Solano-Gonzàlez, J. A. Vendrell, S. Hacot, H. C. Mertani, M. A. Albaret, J.-C. Bourdon, L. Jordan, A. Thompson, Y. Tafer, R. Cong, P. Bouvet, J.-C. Saurin, F. Catez, A.-C. Prats, A. Puisieux, J.-J. Diaz, p53 acts as a safeguard of translational control by regulating fibrillarin and rRNA methylation in cancer. *Cancer Cell* **24**, 318–330 (2013).
56. Y.-C. Hwang, T.-Y. Lu, D.-Y. Huang, Y.-S. Kuo, C.-F. Kao, N.-H. Yeh, H.-C. Wu, C.-T. Lin, NOLC1, an enhancer of nasopharyngeal carcinoma progression, is essential for TP53 to regulate *MDM2* expression. *Am. J. Pathol.* **175**, 342–354 (2009).

57. C. Zhang, C. Yin, L. Wang, S. Zhang, Y. Qian, J. Ma, Z. Zhang, Y. Xu, S. Liu, HSPC111 governs breast cancer growth by regulating ribosomal biogenesis. *Mol. Cancer Res.* **12**, 583–594 (2014).
58. R. A. Shamanna, M. Hoque, T. Pe'ery, M. B. Mathews, Induction of p53, p21 and apoptosis by silencing the NF90/NF45 complex in human papilloma virus-transformed cervical carcinoma cells. *Oncogene* **32**, 5176–5185 (2013).
59. X. Z. Zhou, K. P. Lu, The Pin2/TRF1-interacting protein PinX1 is a potent telomerase inhibitor. *Cell* **107**, 347–359 (2001).

Acknowledgments: We thank R. Lukeis and M. Suter at the Department of Cytogenetics (SydPath), St. Vincent's Hospital, Darlinghurst, New South Wales, Australia, for histological assistance with the tissue microarray. We also thank J. Shohet (Baylor College of Medicine) for providing the SHEP.MYCN3 cells used in this study. **Funding:** This work was supported by program grants from the National Health and Medical Research Council, Australia (grants APP1016699 and APP1085411), Cancer Institute NSW (grant 10/TPG/1-03), Cancer Council NSW (grant PG-11-06), Australian Rotary Health/Rotary Club of Adelaide, Fund for Scientific Research Flanders (FWO), German Cancer Aid (grant 110122), German Ministry of Science and Education (BMBF) as part of the e:Med initiative (grants 01ZX1303A and 01ZX1307D), and Fördergesellschaft Kinderkrebs-Neuroblastom-Forschung e.V. **Author contributions:** M.H. and G.M.M. conceived the project. D.R.C., M.H., and G.M.M. supervised the project. B.B.C., C.B., D.S.Z., T.L., K.V.G., and A.V.G. were advisors for the project. A.O., M.F., J.B., F. Speleman, K.D.P., and A.B. supplied tissues or patient/mouse data for the experiments. D.R.C., J.M., A.J.G., N.I., A.P., M.D.N., M.H., and G.M.M. designed the experiments. D.R.C., J.M., H.K., L.G., J.K., J.T., S. Sutton, S. Syed, A.J.G., N.I., A.B., B.A., Y.S., N.S., D.L., P.Y.K., H.W., A.C., M.R., B.L., F. Salleta, L.M.T., A.P., and G.H. performed the experiments. D.R.C., J.M., L.G., A.J.G., N.I., B.L., and A.P. analyzed the experiments. D.R.C. and G.M.M. wrote the manuscript. J.M., L.G., A.J.G., K.V.G., A.V.G., M.D.N., and M.H. reviewed the manuscript. **Competing interests:** This work was funded in part by grants to K.V.G., A.V.G., M.D.N., and M.H. from Incuron, LLC. K.V.G. and A.V.G. are co-inventors on patents describing CBL0137. M.D.N. and M.H. own some stock in Cleveland BioLabs, which is entitled to a portion of the royalties for sale of Incuron's product, CBL0137. The other authors declare that they have no competing interests. **Data and materials availability:** Gene expression data for neuroblastoma tumors (n = 649) are available at the Gene Expression Omnibus under accession no. GSE45547. All other gene expression data are available at the Gene Expression Omnibus under accession no. GSE71062. CBL0137 is available under a material transfer agreement from Incuron, LLC.

Submitted 23 March 2015
Accepted 26 August 2015
Published 4 November 2015
10.1126/scitranslmed.aab1803

Citation: D. R. Carter, J. Murray, B. B. Cheung, L. Gamble, J. Koach, J. Tsang, S. Sutton, H. Kalla, S. Syed, A. J. Gifford, N. Issaeva, A. Biktasova, B. Atmadibrata, Y. Sun, N. Sokolowski, D. Ling, P. Y. Kim, H. Webber, A. Clark, M. Ruhle, B. Liu, A. Oberthuer, M. Fischer, J. Byrne, F. Saletta, L. M. Thwe, A. Purmal, G. Haderski, C. Burkhart, F. Speleman, K. De Preter, A. Beckers, D. S. Ziegler, T. Liu, K. V. Gurova, A. V. Gudkov, M. D. Norris, M. Haber, G. M. Marshall, Therapeutic targeting of the MYC signal by inhibition of histone chaperone FACT in neuroblastoma. *Sci. Transl. Med.* **7**, 312ra176 (2015).

Science Translational Medicine

Therapeutic targeting of the MYC signal by inhibition of histone chaperone FACT in neuroblastoma

Daniel R. Carter, Jayne Murray, Belamy B. Cheung, Laura Gamble, Jessica Koach, Joanna Tsang, Selina Sutton, Heyam Kalla, Sarah Syed, Andrew J. Gifford, Natalia Issaeva, Asel Biktasova, Bernard Atmadibrata, Yuting Sun, Nicolas Sokolowski, Dora Ling, Patrick Y. Kim, Hannah Webber, Ashleigh Clark, Michelle Ruhle, Bing Liu, André Oberthuer, Matthias Fischer, Jennifer Byrne, Federica Saletta, Le Myo Thwe, Andrei Purmal, Gary Haderski, Catherine Burkhart, Frank Speleman, Katleen De Preter, Anneleen Beckers, David S. Ziegler, Tao Liu, Katerina V. Gurova, Andrei V. Gudkov, Murray D. Norris, Michelle Haber and Glenn M. Marshall

Sci Transl Med **7**, 312ra176312ra176.
DOI: 10.1126/scitranslmed.aab1803

Uncovering the FACTs in neuroblastoma

Neuroblastoma is a common pediatric cancer of the nervous system. It is often difficult to treat, and tumors with amplifications of the *MYC* oncogene are particularly aggressive. Carter *et al*. have identified a histone chaperone called FACT as a mediator of MYC signaling in neuroblastoma and demonstrated its role in a feedback loop that allows tumor cells to maintain a high expression of both MYC and FACT. The authors then used curaxins, which are drugs that inhibit FACT, to break the vicious cycle. They demonstrated that curaxins work in synergy with standard genotoxic chemotherapy to kill cancer cells and treat neuroblastoma in mouse models.